DOE Year 3 (Final) Progress Report

Title: Role of low frequency sea surface temperature modes with a changing climate in modulating Atlantic hurricane activity
Project ID: 0018366

PI: Timothy LaRow
Florida State University

Award Register#: ER65094

DOE Award No. DESC0004969

August 3, 2014

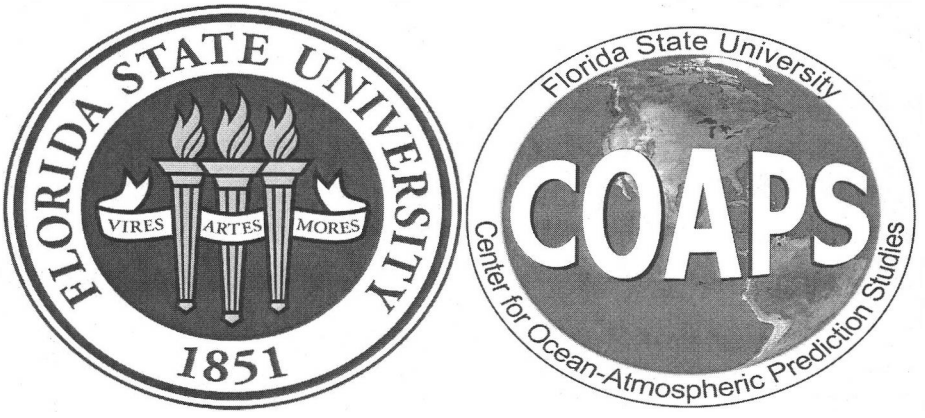

Low Frequency SST Modes and North Atlantic Tropical Cyclone Activity

The SSTs used in our study come from the Community Climate System Model version 4 (CCSM4) (Gent et al 2011) and from the Canadian Centre for Climate Modeling and Analysis (CanESM2) (Chylek et al 2011) climate models from the fifth Coupled Model Intercomparison Project (CMIP5) (Taylor et al 2012). We've examined the tropical cyclones using both the historical simulation that employs volcanic and aerosol forcing as well as the representative concentration pathway 4.5 (RCP4.5). In addition, we've compared the present day North Atlantic tropical cyclone metrics from a previous study (LaRow, 2013) to these climate change experiments. The experimental setup is shown in Table 1. We considered the CMIP5 experiment number '3.2 historical' (Taylor et al, 2011), which provides simulations of the recent past (1850-2005). The second set of CMIP5 SSTs is the RCP4.5 experiment where the radiative forcing stabilizes at 4.5W m^{-2} after 2100 (experiment number 4.1 in Taylor et al 2011).

Model	Historical Climatological SSTs	RCP4.5 Climatological SSTs	RCP4.5 SSTs Positive AMO Phase	RCP4.5 SSTs Negative AMO Phase
CanESM2	10-years	10-years	20-years [2020-2039] 20-years [2080-2099]	20-years [2020-2039] 20-years [2080-2099]
CCSM4	10-years	10-years	20-years [2020-2039] 20-years [2080-2099]	20-years [2020-2039] 20-years [2080-2099]
CFSv1 Bias Corrected SST				13-years [1982-1994]
CFSv1 Bias Corrected SST			15-years [1995-2009]	

Table 1: Experiments

SSTs

Before discussing the projections of tropical cyclone activity in the early and late 21st century the CMIP5 SSTs used in the study is examine. The CanESM2 and CCSM4 model annual SST bias is shown in Figure 1. Figure 1a shows the bias for the CanESM2 model while figure 1b shows the bias for the CCSM4 model. The bias is calculated from the models' historical simulation compared against the ERSSTv3 SST (Smith et al. 2008). The CanESM2 model shows a pronounced cold bias in the central equatorial Pacific along with cold biases in the subtropical gyres. The SST bias in the CCSM4 model is less pronounced compared to the CanESM2 model. The largest cold bias in the tropics is located in the North Atlantic (-1K) while the equatorial Pacific shows a weak cold bias below -0.5K.

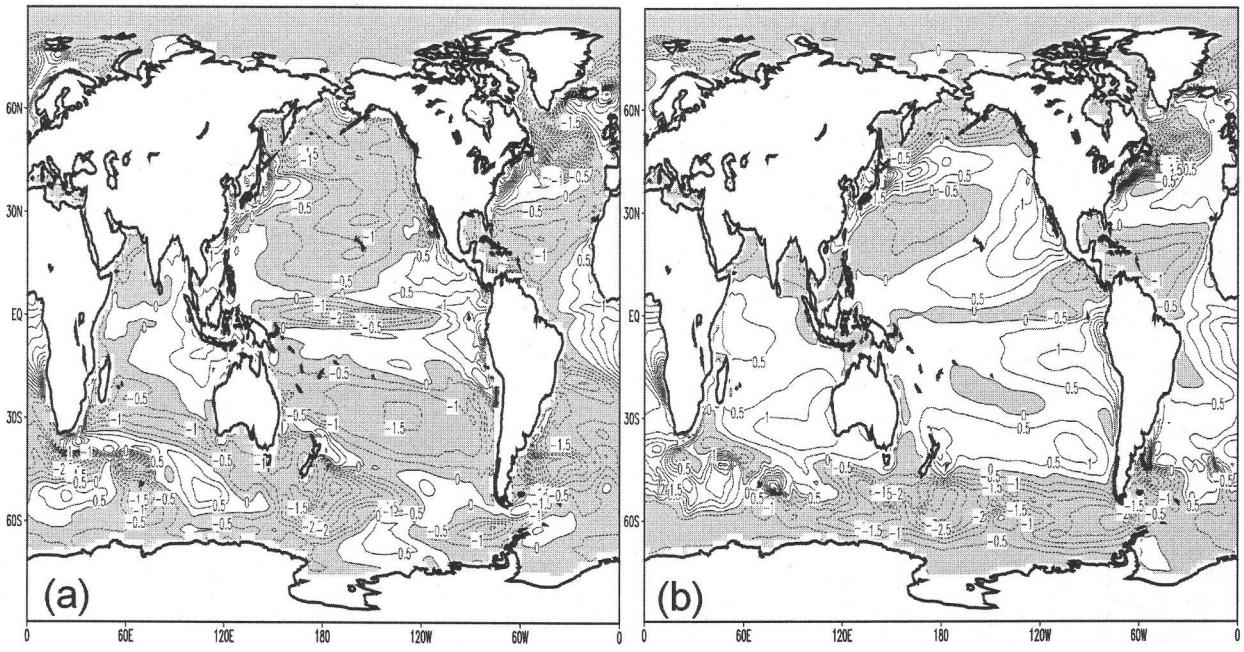

Figure 1 CMIP5 historical simulation annual SST bias with respect to the ERSSTv3 SST 1854-2005. (a) CanESM2, (b) CCSM4. Negative values shaded. Contour interval is 0.5K.

The annual mean SST time series for three selected domains from the CanESM2 and CCSM4 models are shown in Figure 2. The three domains are the Niño-3.4 [190E-240E; 5S-5N], Main Development Region (MDR) [280E-340E; 5N-15N] and the global tropics [30S-30N]. The black lines are the non-bias corrected SSTs from both the historical simulation and the RCP4.5, the red/blue lines show the bias corrected SSTs with the observed positive/negative phase of the AMO imposed (hereafter denoted as AMO+ and AMO-). For reference the green line shows the ERSSTv3 SST since 1940.

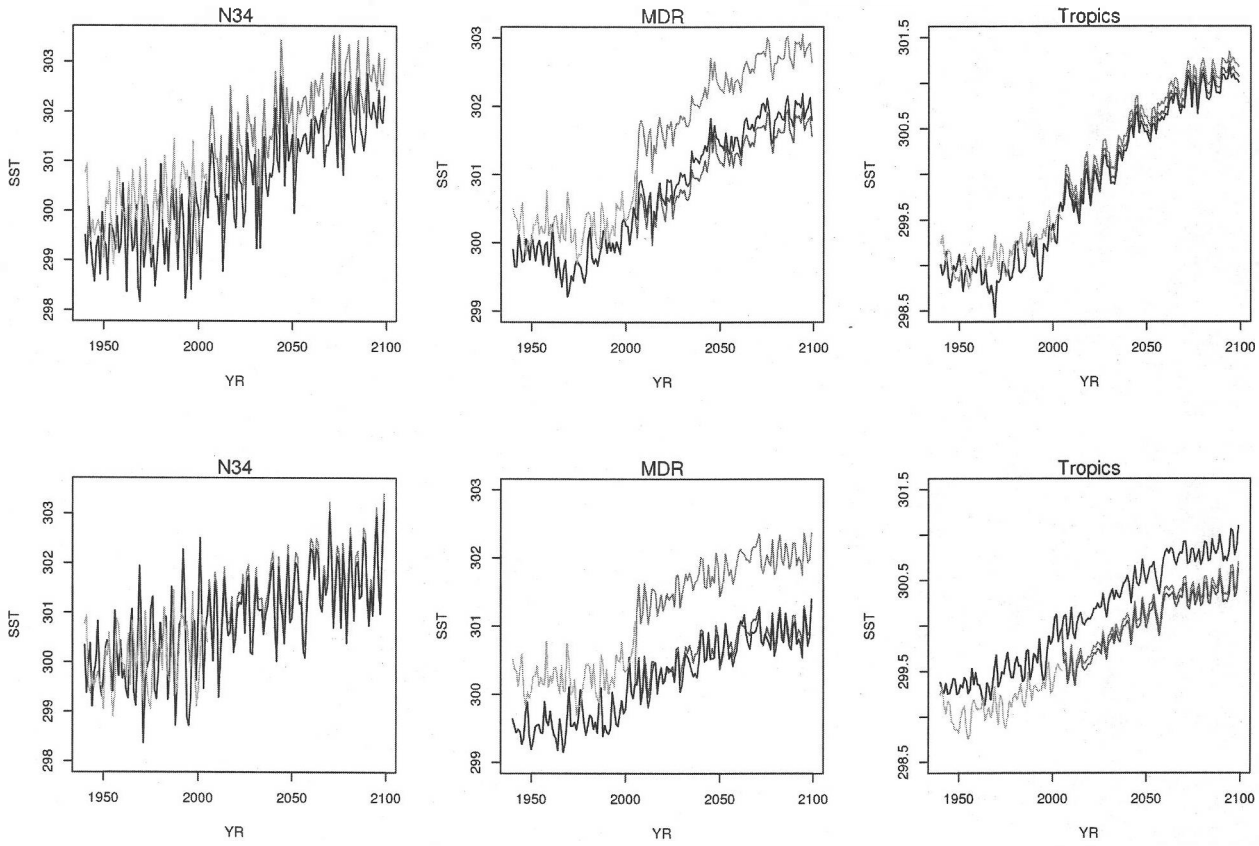

Figure 2 Annual SST time series in the Nino-3.4, main development region and the global tropics. Black lines are the historical and RCP4.5 simulation (not bias corrected). Red lines are the bias corrected SSTs (AMO+); blue lines are the bias corrected SST (AMO-) and the green lines are the ERSSTv3 SSTs since 1940. Top panel is the CanESM2 model. Bottom panel is the CCSM4 model. Unit Kelvin.

The SST warming in the 21st century simulation is clearly evident in all three regions. Both models exhibit larger than observed year-to-year variability in the Niño-3.4 region with the CanESM2/CCSM4 models having standard deviations of 1.2/1.0K while the observed values is 0.6K. In the MDR region the mean difference between the CanESM2 with the AMO+/AMO- and the RCP4.5 simulation is 0.86K/-0.21K. For the CCSM4 model the mean differences in the MDR region between the AMO+/AMO- and the RCP4.5 simulation is 1.15K/0.09K.

Tropical Cyclones

A box whisker plot of the named storms and hurricane counts for the North Atlantic using the modified RCP4.5 SSTs is shown in Figure 3. Also shown in the figure are the counts from a previous experiment where the CFSv1 (Saha et al. 2006) forecast SST were bias corrected before using as a lower boundary condition in the atmospheric model (LaRow, 2013). These bias corrected SSTs are denoted as BC1 and BC2 and correspond to the time periods: 1982-1994 and 1995-2009, respectively, and correspond to the period when the observed AMO was negative and positive (Goldenberg et al. 2001).

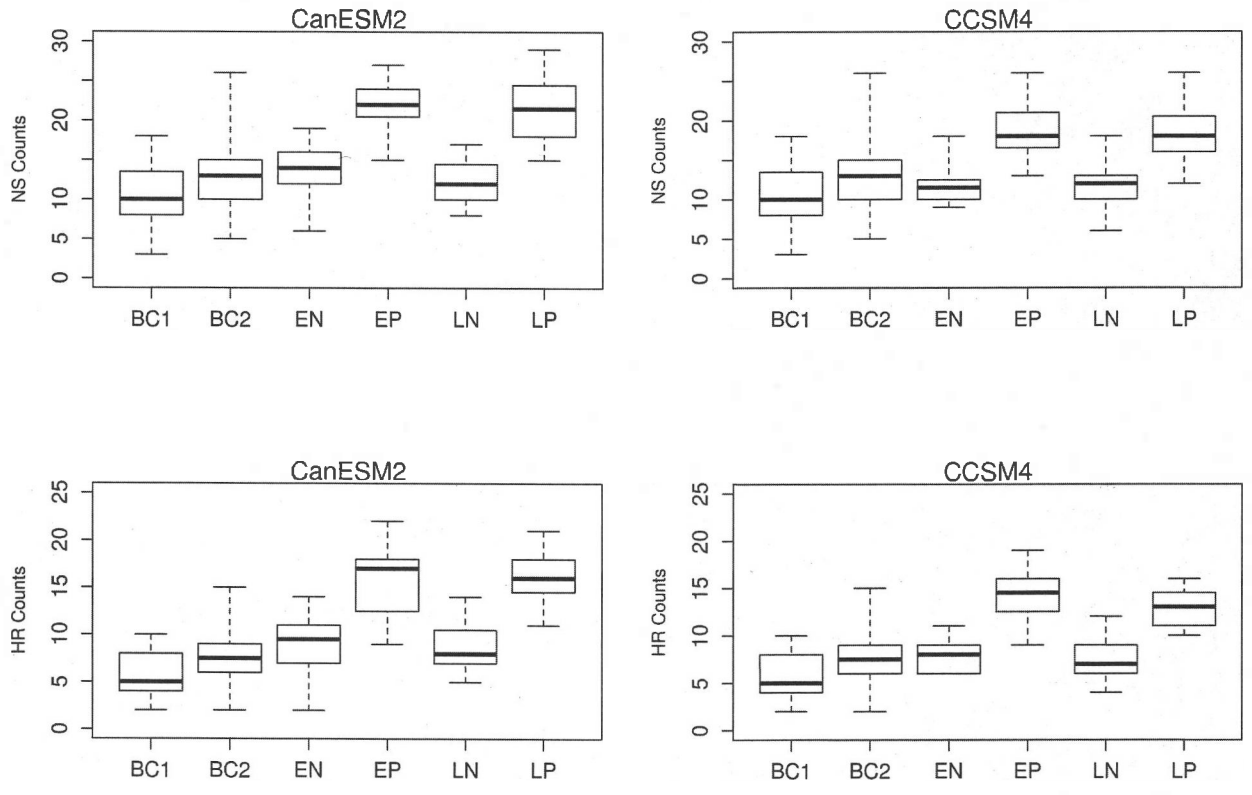

Figure 3 Box whiskers plots of named tropical cyclone and hurricane counts in the North Atlantic. EN and EP denote the early 21st century simulations using the AMO- and AMO+ phases and the LN and LP denote the late 21st century simulations with the AMO-/AMO+ phases.

Throughout the remainder of this progress report the early 21st century simulations with the AMO-/AMO+ phases will be denoted as **EN/EP** and the late 21st century simulations with the AMO-/AMO+ phases will be denoted as **LN/LP**. For both the CanESM2 and CCSM4 AMO+/AMO- simulations the model predicts an overall increase in both named systems and hurricanes compared to the BC1 and BC2 simulations. The increase is greater with the AMO+ simulation compared to the AMO- simulation. For both the early and late 21st century simulations the 25th percentile of the counts for the AMO+ is greater than the 75th percentile of the BC2 simulation while the medians in the AMO- simulations are similar to the BC2 simulation. Averaging the number of hurricanes in the early and late 21st century for both the CanESM2 AMO+ and AMO- simulations yields a 71% increase over the 1982-2009 simulated counts. For the CCSM4 simulation there is a 50% increase in hurricane counts. The percent increase is quantitatively similar to the 61% increase found in Zhao et al. (2009).

Table 2 summarizes the correlations between the interannual variability in the hurricanes and tropical storm counts in the AMO-/AMO+ simulations for both the early and late 21st century simulations with the selected domain average SSTs and wind shear in the MDR. We've found that in general the CanESM2 AMO+/AMO- simulations produced more then twice the number of significant correlations compared to the CCSM4 simulations (28/40 compared to 12/40). In addition we found that the phase of the AMO did not appear to change the number of significant correlations. The relative SST index (Vecchi and Soden 2007) along with the Niño-3.4 SSTs appears to be the best predictors for North Atlantic tropical cyclone activity in our model.

AMO +	Niño-34 SST	MDR SST	AMM	Relative SST	MDR Shear
CanESM HR	**-0.45** (-0.41)	0.24 (0.30)	**0.58** (0.37)	**0.46** (**0.57**)	-0.37 (**-0.41**)
CanESM TS	**-0.47** (**-0.58**)	**0.39** (**0.44**)	**0.44** (0.31)	**0.58** (**0.74**)	**-0.45** (**-0.39**)

AMO -	Niño-34 SST	MDR SST	AMM	Relative SST	MDR Shear
CanESM HR	**-0.62** (-0.18)	0.30 (**0.61**)	**0.52** (**0.52**)	**0.66** (**0.67**)	**-0.59** (-0.30)
CanESM TS	**-0.47** (-0.29)	0.30 (**0.50**)	**0.44** (**0.57**)	**0.53** (**0.69**)	**-0.59** (-0.35)

AMO +	Niño-34 SST	MDR SST	AMM	Relative SST	MDR Shear
CCSM4 HR	-0.09 (0.25)	**0.43** (-0.03)	**0.44** (0.28)	0.31 (0.25)	-0.32 (-0.24)
CCSM4 TS	**-0.44** (**-0.70**)	0.19 (-0.13)	0.28 (0.08)	0.25 (0.28)	**-0.40** (-0.37)

AMO -	Niño-34 SST	MDR SST	AMM	Relative SST	MDR Shear
CCSM4 HR	-0.37 (**-0.45**)	0.05 (0.27)	0.11 (-0.31)	-0.07 (**0.38**)	-0.37 (**-0.53**)
CCSM4 TS	**-0.41** (**-0.71**)	0.02 (0.25)	0.21 (-0.20)	0.03 (**0.56**)	-0.34 (**-0.60**)

Table 2. Correlations of hurricane and tropical storm counts vs. selected SST indices and vertical wind shear for the two SSTs and two phases of the AMO. Values shown in the tables are for the early(late) 21st century simulations. Values shown in bold are significant at the 90% level.

The maximum 10-m wind speed achieved from each tropical cyclone in the North Atlantic from all the simulations is shown in the box whisker plot in Figure 4. The maximum 10-m wind speed obtained by the model simulations is 54 m s^{-1}. This occurs in both the AMO+ and AMO- phases. In the present day climate, BC2 produced a maximum wind speed of 52 m s^{-1}. Overall, regardless of the AMO phase, the tropical cyclone wind speeds increase in the 21st century simulations compared to the model's current climate. The median values in both the CanESM2 and CCSM4 AMO+/AMO- simulations are higher than the BC2 simulation. The median value in the CanESM2 simulations increases as the sea surface temperatures increase. In addition, we find that the model median values for the AMO+ (EP/LP) simulations are higher than the AMO- simulations (EN/LN). This is qualitatively similar to the observations in Goldenberg et al (2001) showing the positive phase of the AMO tends to produce more intense hurricanes (surface wind speeds > 50 ms^{-1}).

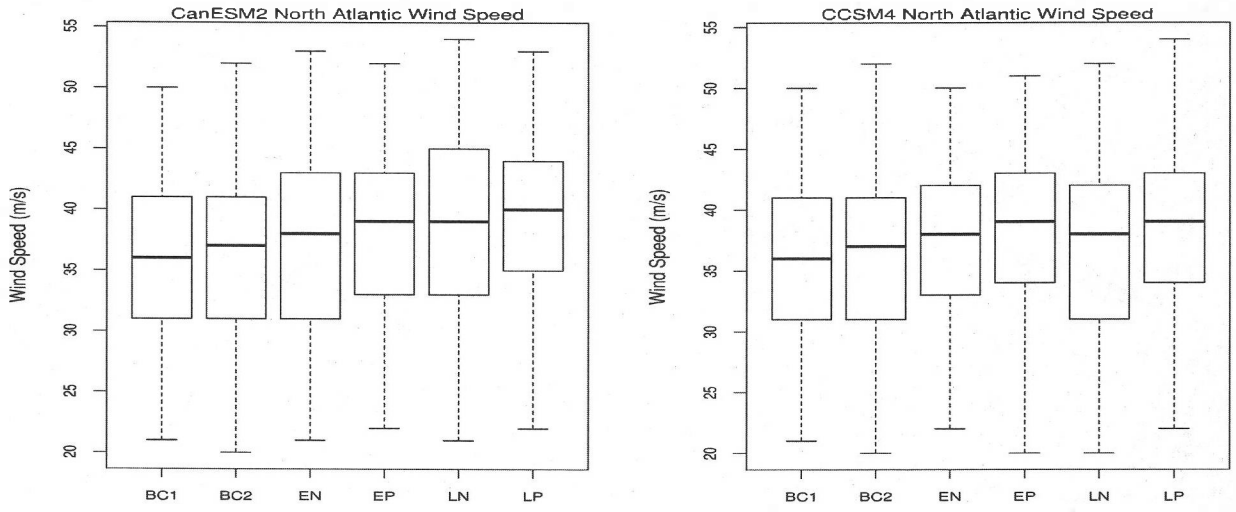

Figure 4 Box whisker plot of 10-m maximum wind speed from each tropical cyclone in the North Atlantic. Units m s^{-1}.

Figure 5 shows the PDFs of the North Atlantic tropical cyclone maximum wind speeds every 6-hours during the lifetime of the storms. Red lines are future projections based on the CanESM2 simulations while the blue lines are the future projections based on the CCSM4 simulations. Solid black lines are the present day model tropical cyclone wind speeds using bias corrected SSTs (1982-1994) and the dashed black lines are the present day model tropical cyclone winds speeds using bias corrected SSTs from 1995-2009.

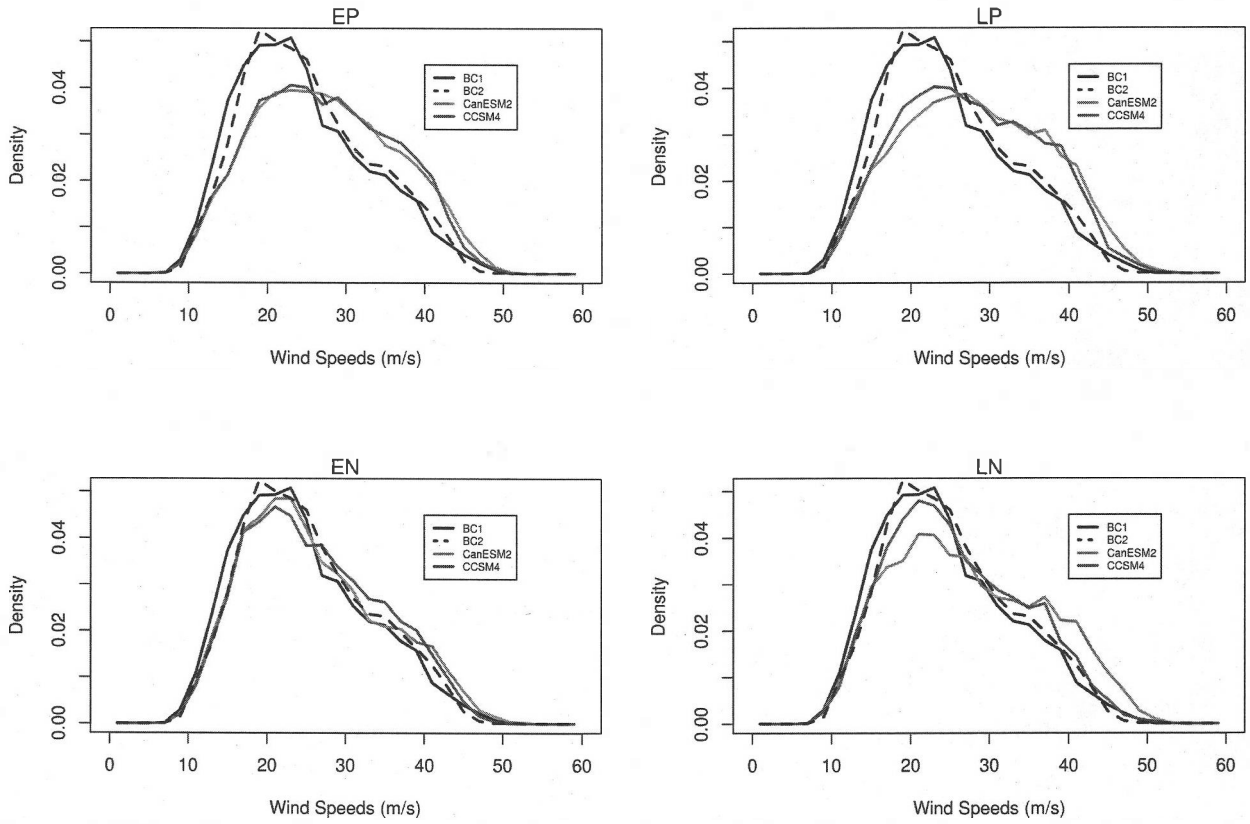

Figure 5 PDF of North Atlantic tropical cyclone wind speeds. Red lines are future projections based on CanESM2 simulations and the blue lines are the future projections based on the CCSM4 simulations. Solid black lines are the present day model tropical cyclone wind speeds using bias corrected SSTs (1982-1994) and the dashed black lines are the present day model tropical cyclone winds speeds using bias corrected SSTs from 1995-2009. Bin width 2 m s^{-1}. Units m s^{-1}.

Figure 6 shows the genesis counts for both the AMO- and AMO+ simulations from the CCSM4 (top panels) and CanESM2 (bottom panels) accumulated over the two 20-year periods. The genesis counts are binned on a 3x3 grid. As already mentioned the positive phase of the AMO produces more tropical systems than the negative phase of the AMO and this is seen in the figure. However, the distribution of the genesis locations in the North Atlantic is different depending upon the choice of SST. The CanESM2 AMO simulations show the majority of genesis occurring within the classical definition of the MDR region, regardless of the phase of the AMO. This result is similar to the results seen in LaRow (2013) and therefore we don't see a climate change signal in the main genesis region in the model. In contrast, the CCSM4 AMO simulations produce two general locations for genesis. The first one located in the MDR region and the second one located slightly pole ward, off the southeast coast of the United States. This secondary location of genesis is a result of SSTs in the negative AMO simulation that is +1K greater than the AMO+ (not shown). In both the CCSM4 and CanESM2 simulations, the mean and median genesis latitude in the negative phase of the AMO is found pole ward of the positive AMO phase with the difference in the average genesis latitude is approximately 4° between the positive and negative AMO phases. We do find that the AMO+ simulations do produce more storm genesis in the Caribbean and Gulf of Mexico compared to the AMO- simulations. This is especially evident in the CCSM4 simulations. In addition, the AMO+ simulations (both the CCSM4 and CanESM2) produce Cape Verde storms whereas the AMO- simulations do not.

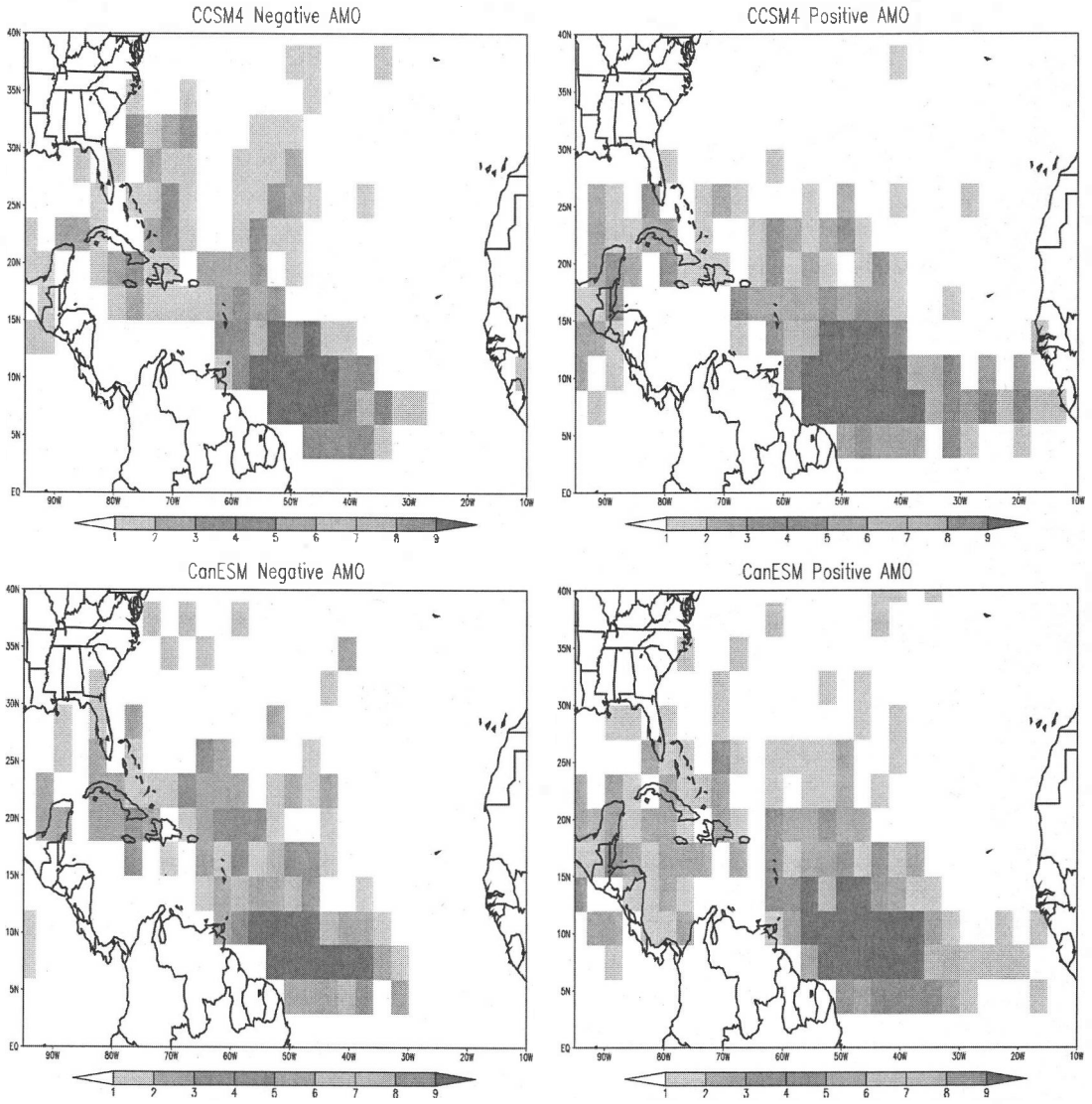

Figure 6 Tropical cyclone genesis densities for CCSM4 (top) and CanESM2 (bottom). Data binned to a 3x3 grid.

In order to examine the changes in landfall/land impacting events in the AMO climate change experiments we've counted the number of 6-hour periods when a tropical cyclone with a the minimum central pressure reached 965 hPa or less for the two phases of the AMO were also examined. The central pressure cutoff of 965 hPa is chosen since it corresponds to CAT3 or greater on the Saffir-Simpson wind damage scale. To identify the land impacting storms of CAT3 or greater, storms with central pressure less than or equal to 965 hPa that are found inside the domain [260W-292W; 25N-50N] are counted. The AMO- simulations were found to produce noticeably fewer hurricanes with central pressures less than 965 hPa impacting the U.S. (between 37-81% fewer) compared to the AMO+ simulations. This pattern of enhanced landfalls (land impacting events), and stronger storms, during the positive AMO phase is noted in the observations (Goldenberg et al. 2001). We also found that the CanESM2 AMO-/AMO+ simulations produced more land impacting events than the CCSM4 simulations, 78% and 34%, respectively. The lack of intense tropical systems in the Gulf of Mexico is more a result of an insufficient number of storms entering or developing in the Gulf of Mexico (LaRow

et al. 2008) rather than a lack of environmental support since maximum potential intensity (Bister and Emanuel 1998) calculations indicate support for intense systems in the Gulf. We are currently investigating this issue.

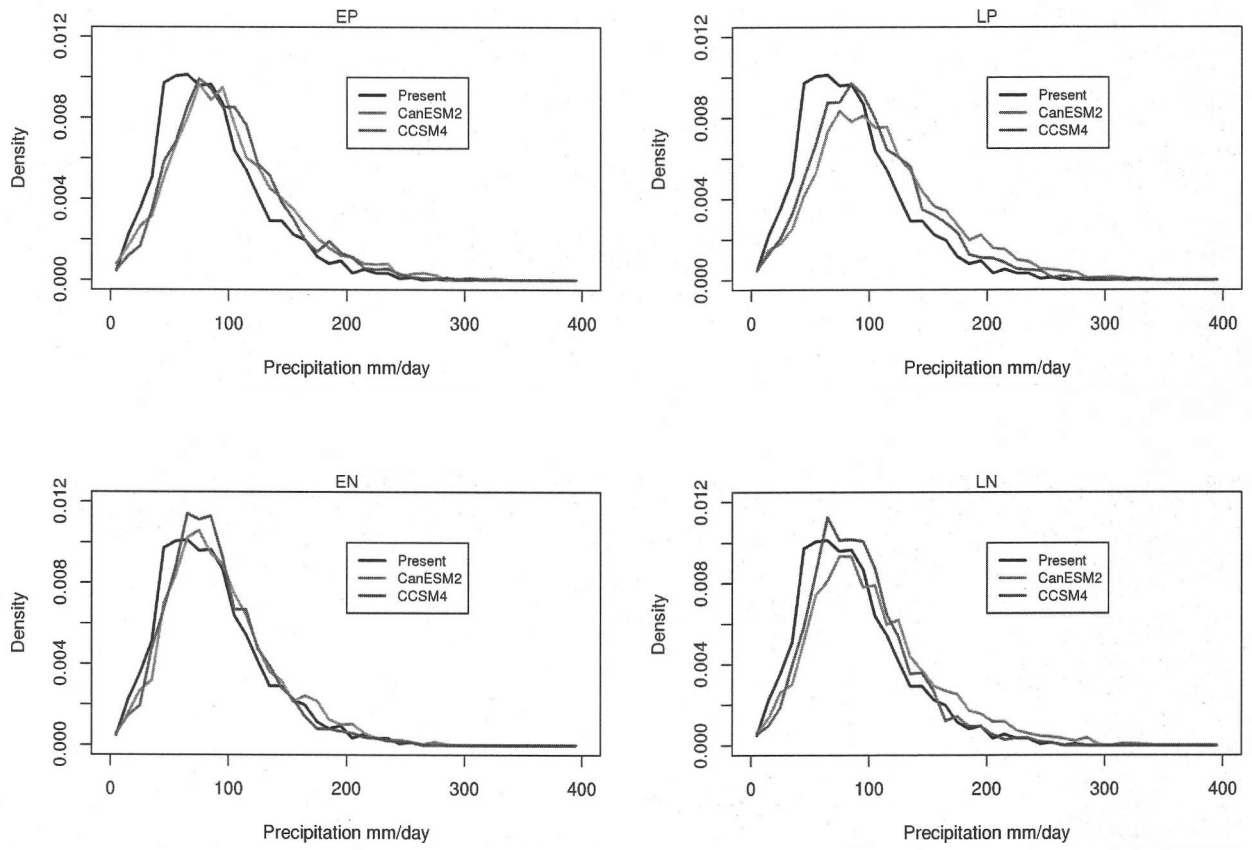

Figure 7 PDF of the North Atlantic tropical cyclone area averaged precipitation.

Figure 7 shows the PDFs of the North Atlantic tropical cyclone area averaged precipitation. Black lines show the precipitation in the current climate [1982-2009] from the BC1 and BC2 simulations and the red/blue lines show the storm precipitation associated with the CanESM2/CCSM4 simulations in the AMO+ and AMO- simulations. The area averaged precipitation is computed using a 2° radius centered on the tropical cyclones minimum central pressure. The tropical cyclone mean precipitation in the current climate from BC1 and BC2 is 86 mm day^{-1}. The mean tropical cyclone precipitation in the AMO+/AMO- simulations increases to 101 mm day^{-1} in the CCSM4 LP simulation and up to 112 mm day^{-1} in the CanESM2 LP simulation. The mean North Atlantic tropical cyclone precipitation from all the AMO simulations is statistically different at the 95% level compared to the current climate simulations.

ENSO/Southeast Precipitation in CMIP5 Historical Simulations

Winter precipitation anomalies over the Southeast United States (SEUS) are strongly modulated by ENSO (e.g. Ropelewski and Halpert, 1986, 1987; Kiladis and Diaz, 1987; Higgins et al 2000; Markowski and North 2003). Typical El Niño winters are associated with relatively frequent Gulf of Mexico storms (Eichler and Higgins 2006) and consequent cooler surface temperatures and an increase in regional precipitation. Conversely, La Niña winters see fewer storm passages and are therefore

generally warmer and drier. The strength of the relationship between ENSO and regional precipitation anomalies is well documented in the literature, and has been widely utilized by planners in realms such as agriculture, forestry and utilities. A scatter plot of observed (1948-2004) DJF area-averaged precipitation anomalies for the SEUS versus the contemporaneous Niño-3.4 temperature anomalies (Fig 8) illustrates the strength of this relationship. The correlation between the two time series is 0.65. While this is clearly statistically significant (based on Student's t-test), a non-trivial fraction of precipitation variance remains unexplained by ENSO, and must be attributed to other modes of large-scale variability.

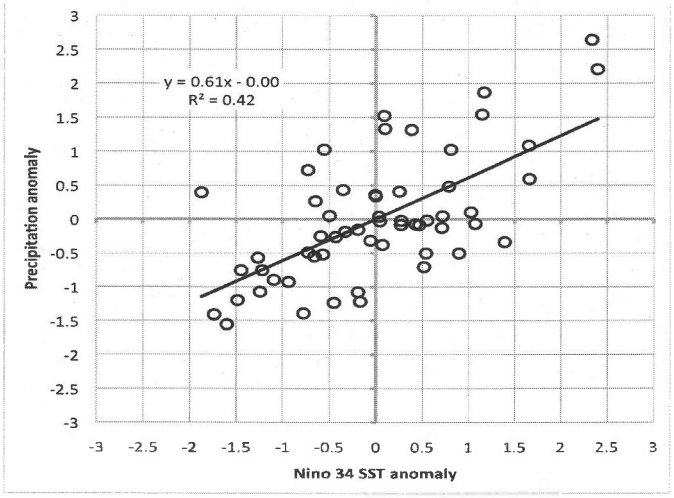

Figure 8 Scatter plot of observed (1948-2004) SEUS DJF precipitation anomalies [mm day^{-1} K^{-1}] vs. the contemporaneous Niño-3.4 SST anomalies [K]. The correlation coefficient between the two series is the square root of R^2 (marked on the plot) or, in this case, 0.65.

Since such a large proportion of the SEUS' winter precipitation variability is explained by ENSO, the degree to which contemporary climate models are capable of simulating this relationship may be essential in determining the utility of such models for regional climate change adaptation planning.

To address this question we calculated the correlation between the area-averaged SEUS DJF precipitation anomalies and the Niño-3.4 SST anomalies for the same period (1948-2004) from the CMIP5 historical simulations for all available ensemble members. The slopes of the linear fits and the R^2 values for all model runs are summarized in Table 3.

Model	Ensemble Member	Slope [mm day^{-1} K^{-1}]	R^2
OBS	N/A	***0.61***	***0.42***
CanESM2	r1	0.57	0.62
	r2	-0.13	0.03
	r3	-0.04	0.00
	r4	0.15	0.04
	r5	0.09	0.02
CNRM-CM5	r1	0.49	0.59
	r2	0.44	0.43
	r3	0.51	0.52
	r4	0.47	0.50
	r5	0.46	0.50

CSIRO-Mk3-6-0	r1	0.60	0.29
	r2	0.44	0.10
	r3	0.95	0.43
	r4	0.81	0.33
	r5	0.73	0.30
GFDL	r1	0.08	0.02
GISS-E2-H	r1	0.47	0.28
	r2	0.28	0.06
	r3	0.40	0.16
	r4	0.15	0.02
	r5	0.33	0.18
GISS-E2-R	r1	0.41	0.26
HadCM3	r1	0.26	0.22
	r2	0.16	0.07
	r3	0.31	0.19
	r4	0.32	0.27
	r5	0.03	0.00
	r6	0.29	0.30
	r7	0.20	0.11
	r8	0.30	0.24
	r9	0.28	0.23
	r10	0.38	0.21
Inmcm4	r1	0.13	0.03
MIROC5	r1	0.52	0.80
	r2	0.39	0.56
	r3	0.42	0.53
	r4	0.46	0.57
MPI-ESM-LR	r1	0.29	0.17
	r2	0.30	0.18
	r3	0.30	0.21
MRI-CGCM3	r1	0.73	0.38
	r2	0.86	0.48
NorESM1-M	r1	0.41	0.46
	r2	0.49	0.54
	r3	0.36	0.44

Table 3: Slope [mm day^{-1} K^{-1}] of the linear fit and R^2 between SEUS DJF precipitation anomaly and contemporaneous Niño-3.4 SST anomaly from observations and model historical runs for the period 1948-2004.

The majority of model runs show a realistic relationship between the SEUS DJF precipitation anomalies and Niño-3.4 SST anomalies. A few exceptions, with $R^2<0.1$ (correlation coefficient <0.32) are however present. In four out of the five CanESM2 model runs the two time series are practically uncorrelated; similar weak to absent correlation is present in the GFDL model run, two of the five GISS-E2-H model runs, two of the ten HadCM3 model runs, and the Inmcm4 model run.

The finding that in several instances within the same model some ensemble members show significant correlations between SEUS DJF precipitation and Niño-3.4 SST, while other ensemble members show lack of correlation is surprising, since the underlying physical processes should be the same. This suggests a strong internal variability of the strength of the relationship between Nino 34 SSTs and SEUS precipitation as simulated by these models. This may be at least partially explained by the

models' internal variability of multidecadal modes of Northern Pacific variability that have been found to modulate the strength of ENSO teleconnections (Latif and Barnett, 1996; Gershunov and Barnett, 1998; Diaz et al. 2001) or Atlantic Multidecadal variability (Enfield et al., 2001).

The implications of our findings are that model projections of precipitation changes will have to be treated with caution and the physical mechanisms governing the large-scale influence on a region of interest, such as the SEUS, must be carefully explored within each model's context.

References

Bell, G., and M. Chelliah, 2006: Leading Tropical Modes Associated with Interannual and Multidecadal Fluctuations in North Atlantic Hurricane Activity. J. Climate, 19, 590-612.

Bengtsson, L., et al., 2007: How may tropical cyclones change in a warmer climate. *Tellus*, **59A**, 539-561.

Bister, M., and K. Emanuel, 1998: Dissipative heating and hurricane intensity. *Meteor. Atmos. Phys.*, **55**, 233–240.

Chylek P, Li J, Dubey M, Wang M, Lesins G, 2011: Observed and model simulated 20th century arctic temperature variability: Canadian earth system model canesm. *Atmos Chem Phys Discuss*, 11: 22,8932290, DOI f10.5194/acpd-11-22893-201g

Diaz H. F., M.P. Hoerling and J.K. Eischeid, 2001: ENSO variability, teleconnections and climate change. *Int. J. Climatology* **21**, 1845-1862.

Eichler, T., and W. Higgins, 2006: Climatology and ENSO-related variability of North American extratropical cyclone activity. *J. Climate*, **19**, 2076–2093.

Elsner, J. B., A. A. Tsonis, and T. H. Jagger, 2006: High frequency variability in hurricane power dissipation and its relationship to global temperature, *Bull. Am. Meteorol. Soc.*, **87**, 763–768.

Elsner, J., 2006: Evidence in support of climate change-Atlantic hurricane hypothesis. *Geophys. Res. Lett.*, **v33**, L16705,doi:10.1029/2006GL026869.

Enfield D. B., A.M. Mestas-Nunez and P.J. Trimble, 2001: The Atlantic multidecadal oscillation and its relation to rainfall and river flows in the continental US. *Geophys. Res. Lett.*, **28**, 2077-2080.

Gent P. R., et.al. 2011: The Community Climate System Model version 4. *J. Climate*, doi: 10.1175/2011JCLI4083.1

Gershunov A. and T. P. Barnett, 1989: Interdecadal modulation of ENSO teleconnections. *Bull. Amer. Meteor. Soc.,* **79**, 2715-2725.

Gillett, N., P. Scott and D. Santer, 2008: Attribution of cyclogenesis region sea surface temperature change to anthropogenic influence. *Geophys. Res. Lett.* **35**, L09707.

Goldenberg, S., C.W. Landsea, A.M. Mestas-Nuñez, and W.M. Gray, 2001: The recent increase in Atlantic hurricane activity: Causes and implications, *Science*, **293,** 474-479.

Higgins R.W., A. Leetma, Y. Xue and A. Barnston, 2000: Dominant factors influencing the seasonal predictability of US precipitation and surface air temperature. *J. Climate* **13**, 3994–4017.

Karl, T. E., et al. (eds) 2008: Weather and Climate Extremes to a Changing Climate. Regions of Focus: North America, Hawaii, Caribbean, and Pacific Islands. (US Climate Change Science Program and Subcommittee on Global Climate Research. Department of Commerce, NOAA National Data Center.

Kiladis, G. N, and H. F. Diaz, 1989: Global climate extremes associated with extremes of the Southern oscillation. *J. Climate*, **2**, 1069–1090.

Knutson, T., J. McBride, J. Chan, K. A. Emanuel, G. Holland, C. Landsea, Isaac M. Held, J. Kossin, A. K. Srivastava, and M. Sugi, 2010: Tropical cyclones and climate change. *Nature Geoscience*, **3**, DOI:doi:10.1038/ngeo779

LaRow, T. E., Y. K. Lim, D. W. Shin, E. Chassignet and S. Cocke, 2008: Atlantic Basin Seasonal Hurricane Simulations. *J. Climate*, **21**, 3191-3206.

LaRow, T. E., L. Stefanova, D.W. Shin, and S. Cocke, 2010: Seasonal Atlantic Tropical Cyclone Hindcasting/Forecasting using Two Sea Surface Temperature Datasets. *Geophys. Res. Lett.*, **37**, L02804, doi:10.1029/2009GL041459.

LaRow, T. E., 2013: The Impact of SST Bias Correction on North Atlantic Hurricane Retrospective Forecasts. *Mon. Wea. Rev.*, **141**, 490–498. doi:10.1175/MWR-D-12-00152.1

Latif, M. and T. P. Barnett, 1996: Decadal Climate Variability over the North Pacific and North America: Dynamics and Predictability. *J. Climate*, **9**, 2407-2423.

Mann, M. and K. Emanuel, 2006: Atlantic hurricane trends linked to climate change. *Eos Trans. Am.*

Geophys. Union, **87**, 233.

Markowski, G. R. and G. R. North 2003: Climatic influence of sea surface temperature: evidence of substantial precipitation correlation and predictability. *J. Hydromet.*, **4**, 856–877.

Rayner, N. A., D.E. Parker, E.B. Horton, C.K. Folland, L.V. Alexander, D.P. Rowell, E.C. Kent, A. Kaplan, 2003: Global analyses of sea surface temperature, sea ice, and night marine air temperature since the late nineteenth century *J. Geophys. Res.*, **108**, No. D14, 4407 10.1029/2002JD002670

Ropelewski C. F. and M. S. Halpert, 1986: North American precipitation and temperature patterns associated with the El Nino/SouthernOscillation (ENSO). *Mon. Wea. Rev.*, **114**, 2352–2362.

Ropelewski C. F. and M. S. Halpert, 1987: Global and regional scale precipitation patterns associated with the El Nino/Southern Oscillation. *Mon. Wea. Rev.*, **115**, 1606–1626.

Saha, S., and co-authors, 2006: The Climate Forecast System at NCEP. *J. Climate*, **19**, 3483-3517.

Santer, B. and co-authors, 2006: Forced and unforced ocean temperature changes in Atlantic and Pacific tropical cyclogenesis regions. *PNAS*, **103**, 13905-13910.

Smith, T., R. Reynolds, T. Peterson, and J. Lawrimore, 2008: Improvements to NOAA's historical merged land-ocean surface temperature analysis (1880-2006). *J. Clim.*, **21**, 2283-2296.

Swanson, K. L., 2008: Nonlocality of Atlantic tropical cyclone intensities, *Geochem. Geophys. Geosyst.*, **9**, Q04V01 doi:10.1029/2007GC001844.

Taylor, K., R. Stouffer, G. Meehl, 2012: An overview of CMIP5 and the experiment design. *Bull. Amer. Meteorol. Soc.*, **93**, 485-498.

Trenberth, K. E. and D. Shea, 2006: Atlantic hurricanes and natural variability in 2005. *Geophys. Res. Lett.*, **33**, L12704, doi:10.1029/2006GL026894.

Vecchi, G. and B. Soden, 2007: Effect of remote sea surface temperature change on tropical cyclone potential intensity. *Nature*, **450**, 1066-1070.

Vecchi, G., K. L. Swanson, and Brian J. Soden, 2008: Whither Hurricane Activity? *Science*, *322 (5902), 687-689. DOI:10.1126/science.1164396*

Villarini, G. and G. Vecchi, 2012: Twenty-first-century projections of North Atlantic tropical storms from CMIP5 models, *Nature Climate Change*, **2**, 604-607.

Walsh, K., M. Fiorino, C. Landsea and K. McInnes, 2007: Objectively-determined resolution-dependent threshold criteria for the detection of tropical cyclones in climate models and reanalyses. *J. Clim.*, **20**, 2307-2314.

Zhao, M., I. Held, S.-J. Lin, G. Vecchi, 2010: Simulations of global hurricane climatology, interannual variability, and response to global warming using a 50km resolution GCM. *J. Clim.*, **22**, 6653-6678.